

Dealing with Suboptimality in Multistep Model Predictive Control for Transient Operations

Roky Baidya*, Ricardo P. Aguilera†, Petros Karamanakos‡, Pablo Acuna§, Christian Rojas¶,
Tobias Geyer||, and Dylan D.-C. Lu†

*School of Electrical Eng. &, Telecommunication, Chittagong University of Eng. & Technology, Chittagong, Bangladesh

†School of Electrical and Data Engineering, University of Technology Sydney, Sydney, Australia,

‡ Faculty of Information Technology and Communication Sciences, Tampere University of Technology, Tampere, Finland

§Department of Industrial Technologies, University of Talca, Curico, Chile

¶Departamento de Ingeniería Electrónica, Universidad Técnica Federico Santa María, Valparaíso, Chile

||ABB Corporate Research Center, Baden-Dättwil, Switzerland

Email: roky.baidya@ieee.org

Abstract—Recently, a computational issue of sphere decoding algorithm (SDA) during transient operation of multistep model predictive control has been addressed in [1] and achieved its real-time implementation in [2] for a medium-voltage electrical drive system. This is achieved by projecting the unconstrained solution onto the *convex-hull* of the finite control set during transient operation. Therefore, a new initial sphere that guarantees feasibility and includes a significant smaller number of candidate solutions is obtained. This reduces the computation time required to solve the optimization problem. However, the reduction of the computational burden comes at the expense of (mild) suboptimal results [3]. This paper analyses the possibility to obtain a suboptimal solution by the SDA based optimization during transient operation. To deal with this suboptimality issue, this work explores the possibility to enlarge the *convex-hull*, whose size is by definition tied to the original finite control set. Therefore, in this work, the *convex-hull* is treated as a SDA initialization parameter during transient operation. As will be demonstrated, enlarging the *convex-hull* size reduces the possibility to obtain a suboptimal solution during the transient operation retaining, thus, the optimality during the whole converter operation.

Index Terms—Predictive Control, Long Prediction Horizon, Sphere Decoder, Transient Operation, Suboptimality

I. INTRODUCTION

In recent decades, model predictive control (MPC) has paved its way in becoming one of the most attractive control alternatives for power electronics converters and electrical drives [4]. In MPC, an optimal control problem can be formulated by considering the physical limits of the system and, as a result, several constraints and nonlinearities can be included to achieve the best possible outcome. These features of MPC, combined with the available computational power, justify its widespread acceptance from the power electronic community.

Among the MPC families, the finite control set MPC (FCS-MPC) is most widely utilized. In this strategy, the optimization and modulation problem are formulated in one stage; thus, no modulator is needed. However, performing the optimization is still computationally challenging as the number of control inputs or the length of the prediction horizon increases. As

reported recently, multistep MPC can improve the system performance [5]–[7] when compared to its horizon-one counterpart. However, the computational challenges for prediction horizons longer than one are significant. Moreover, the use of an exhaustive search algorithm (ESA)—according to which all candidate solutions are enumerated to conclude to the optimal one—further aggravate these challenges. This is due to the fact that the number of candidate solutions increases exponentially with the prediction horizon steps, rendering ESA computationally intractable.

To achieve real-time implementation of multistep MPC, the sphere decoding algorithm (SDA), originally introduced in the field of communications, can be adapted to solve optimal control problem associated to multistep MPC for power converters and drives [6]–[8]. SDA is an efficient optimization algorithm for quadratic integer optimal problems, which can be used to optimally obtain the converter switch position. This is achieved by setting an *initial sphere* centered on the unconstrained optimal solution and with a radius defined by a good initial input candidate. Thus, any input combination from the FCS that lies outside the sphere is discarded from evaluation. Therefore, the computational efficiency of the SDA is directly associated to the initial sphere. Nevertheless, during transient operation, the unconstrained solution can be placed far from the FCS, yielding to a large initial sphere, which increases the computational time required by the SDA to obtain the optimal solution.

To overcome this issue, an interesting solution was originally proposed in [1]. Therein, a *convex hull* of the FCS was used to discriminate between steady-state and transient operation. In doing so, if the unconstrained optimal solution lies inside the *convex hull* then, the SDA is performed as usual. Conversely, whenever the unconstrained optimal solution lies outside the *convex hull*, it is considered as transient operation. In that case, it is proposed in [1] to project the unconstrained optimal solution onto the *convex hull* and use this projection as center for the initial sphere. Consequently, a new initial sphere that guarantees feasibility and includes a significant smaller

number of candidate solutions is obtained. This reduces the computation time required to solve the optimization problem. This idea has been adopted in [2], [3] for multistep MPC formulated for medium-voltage electrical drive systems. Importantly, the reduction of the computational burden comes at the expense of (mild) suboptimal results [3], since the optimal problem considering the projection differs from the original one.

The paper at hand analyses the possibility to obtain a suboptimal solution by the SDA-based optimization during transient operation. To deal with this suboptimality issue, this work explores the possibility to enlarge the *convex-hull*, whose size is by definition tied to the original finite control set. Therefore, in this work, the *convex-hull* is treated as a SDA initialization parameter during transient operation. As will be demonstrated, enlarging the *convex-hull* size reduces the possibility to obtain a suboptimal solution during the transient operation retaining, thus, the optimality during the whole converter operation. To validate this proposal, an induction motor drive system is chosen as a case study. Simulation results are presented to verify the effectiveness of enlarging the *convex-hull* size, allowing SDA to preserve optimality for the whole range of operating points when using multistep MPC with prediction horizon as long as $N = 10$ steps. Finally, experimental results of the closed-loop system behavior using multistep MPC with $N = 4$ and SDA with enlarged *convex-hull* are also provided.

II. OPTIMAL CONTROL PROBLEM OF IM DRIVE

The predictive controller for an induction machine (IM) drive system here follows the cascaded structure of the field oriented control (FOC), where the electromagnetic system is controlled by a model predictive current control (MPCC) and classical proportional-integral (PI) controllers govern the mechanical system as shown in Fig. 1. The discrete-time state-space model of the IM drive system is formed as

$$\mathbf{x}(k+1) = \mathbf{A}(k)\mathbf{x}(k) + \mathbf{B}\mathbf{u}(k) \quad (1a)$$

$$\mathbf{y}(k) = \mathbf{C}\mathbf{x}(k) \quad (1b)$$

where the state vector, $\mathbf{x} = [i_{s\alpha} \ i_{s\beta} \ \psi_{r\alpha} \ \psi_{r\beta}]^T \in \mathbb{R}^4$, consists of the stator currents and the rotor fluxes in $\alpha\beta$ -framework, while the stator current is the output variable, i.e., $\mathbf{y} = [i_{s\alpha} \ i_{s\beta}]^T \in \mathbb{R}^2$. Finally, the control input vector, $\mathbf{u} = [\mu_a \ \mu_b \ \mu_c]^T \in \mathcal{U} = \mathbb{V}^3$, is composed of the inverter voltage levels, $\mu_\chi, \forall \chi \in \{a, b, c\}$, where $\mu_\chi \in \mathbb{V} = \{-1, 0, 1\}$ for a three-level inverter, and the system matrices (\mathbf{A} , \mathbf{B} and \mathbf{C}) are obtained from the IM drive system model [2]. The latter are summarized in Remark 1.

The main objective of MPCC is for the output variables \mathbf{y} (i.e., the stator currents) to track their references \mathbf{y}^* , while maintaining a low inverter switching frequency. At each time step k , the objectives are mapped into a cost function over a finite prediction horizon N as

$$J_N(k) = \sum_{\ell=k}^{k+N-1} \|\mathbf{y}(\ell+1) - \mathbf{y}^*(\ell+1)\|_2^2 + \lambda_u \|\Delta \mathbf{u}(\ell)\|_2^2 \quad (2)$$

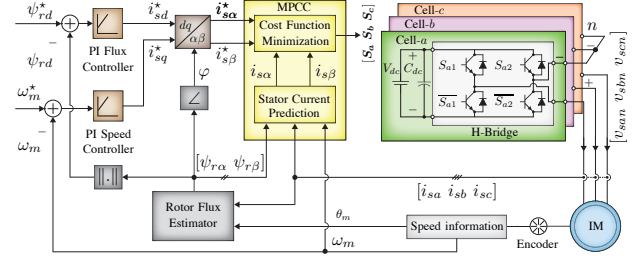


Fig. 1. A cascaded FOC control structure with speed and flux outer control loop and MPCC inner control loop governing an IM fed by a three-phase three-level H-Bridge inverter.

where the first term penalizes the stator current tracking error and the second term ($\Delta \mathbf{u}(\ell) = \mathbf{u}(\ell) - \mathbf{u}(\ell - 1)$) is related to the switching effort. Furthermore, the weighting factor, $\lambda_u > 0$, adjusts the trade-off between these two control targets. Then, the optimal control input sequence, $\mathbf{U}_{\text{opt}}(k) = [\mathbf{u}_{\text{opt}}(k) \ \dots \ \mathbf{u}_{\text{opt}}^T(k + N - 1)]^T$, is obtained by solving the following optimization problem

$$\mathbf{U}_{\text{opt}}(k) = \arg \min_{\mathbf{U}(k)} \{J_N(k)\} \quad (3a)$$

$$\text{subject to: } \mathbf{x}(\ell + 1) = \mathbf{A}(k)\mathbf{x}(\ell) + \mathbf{B}\mathbf{u}(\ell), \quad \mathbf{y}(\ell) = \mathbf{C}\mathbf{x}(\ell) \quad (3b)$$

$$\mathbf{U}(k) \in \mathbb{U} \quad (3c)$$

$$\|\Delta \mathbf{u}(\ell)\|_\infty \leq 1, \quad \forall \ell \in k, \dots, k + N - 1, \quad (3d)$$

where, (3b) is the system constraint given by (1), (3c) restricts the control input sequences, $\mathbf{U}(k) = [\mathbf{u}^T(k) \ \dots \ \mathbf{u}^T(k + N - 1)]^T$, that belong to the FCS, $\mathbb{U} = \mathbb{V}^{\zeta=3N}$, and (3d) is the transition voltage level constraint which is limited to one, in order to avoid high dv/dt ratings [4]. Normally, transition in any voltage level becomes more than one (i.e. violates (3d)) during the transients and/or worst case condition of the steady-states [9].

Remark 1. Considering the stator currents ($\mathbf{i}_s = [i_{s\alpha} \ i_{s\beta}]^T$), the rotor fluxes ($\psi_r = [\psi_{r\alpha} \ \psi_{r\beta}]^T$) and the rotor's speed ω_m as the state-variables, the continuous-time state equations of the IM drive system can be expressed as

$$\frac{d\mathbf{i}_s}{dt} = -\frac{1}{\tau_\sigma} \mathbf{i}_s + \frac{k_r}{R_\sigma \tau_\sigma} \begin{bmatrix} \frac{1}{\tau_r} & \omega_m \\ -\omega_m & \frac{1}{\tau_r} \end{bmatrix} \psi_r + \frac{1}{R_\sigma \tau_\sigma} \mathbf{v}_s \quad (4a)$$

$$\frac{d\psi_r}{dt} = \frac{L_m}{\tau_r} \mathbf{i}_s - \begin{bmatrix} \frac{1}{\tau_r} & \omega_m \\ -\omega_m & \frac{1}{\tau_r} \end{bmatrix} \psi_r \quad (4b)$$

$$J_m \frac{d\omega_m}{dt} = -f_m \omega_m + \mathcal{T}_e - \mathcal{T}_l \quad (4c)$$

where $\tau_r = \frac{L_r}{R_r}$, $k_r = \frac{L_m}{L_r}$, $R_\sigma = R_s + R_r k_r^2$, $L_\sigma = L_s - k_r^2 L_r$, and $\tau_\sigma = \frac{L_\sigma}{R_\sigma}$ stand for rotor time constant, rotor coupling factor, equivalent resistance, total leakage inductance, and transient-stator-time constant, respectively, see [10]. Addi-

tionally, \mathcal{T}_l is the mechanical load torque, and \mathcal{T}_e is the electromagnetic torque given by

$$\mathcal{T}_e = \frac{3}{2} n_p \frac{L_m}{L_r} (\psi_{r\alpha} i_{s\beta} - \psi_{r\beta} i_{s\alpha}) \quad (5)$$

where R_s (R_r), L_s (L_r), L_m , f_m , and n_p stand for stator (rotor) resistance, stator (rotor) inductance, magnetizing inductance, friction coefficient, and number of pole pairs, respectively. According to the MPCC scheme in $\alpha\beta$ -framework, the continuous-time state-space model becomes

$$\frac{d\mathbf{x}(t)}{dt} = \mathbf{A}_c(t)\mathbf{x}(t) + \mathbf{B}_c\mathbf{u}(t), \quad \mathbf{y}(t) = \mathbf{C}\mathbf{x}(t) \quad (6)$$

where

$$\begin{aligned} \mathbf{A}_c(t) &= \begin{bmatrix} -\frac{1}{\tau_\sigma} & 0 & \frac{k_r}{R_\sigma \tau_\sigma \tau_r} & \frac{k_r \omega_m(t)}{R_\sigma \tau_\sigma} \\ 0 & -\frac{1}{\tau_\sigma} & -\frac{k_r \omega_m(t)}{R_\sigma \tau_\sigma} & \frac{k_r}{R_\sigma \tau_\sigma \tau_r} \\ \frac{L_m}{\tau_r} & 0 & -\frac{1}{\tau_r} & -\omega_m(t) \\ 0 & \frac{L_m}{\tau_r} & \omega_m(t) & -\frac{1}{\tau_r} \end{bmatrix}, \\ \mathbf{B}_c &= \frac{V_{dc}}{R_\sigma \tau_\sigma} \mathbf{C}^T \mathbf{c}_t, \quad \mathbf{C} = \begin{bmatrix} 1 & 0 & 0 & 0 \\ 0 & 1 & 0 & 0 \end{bmatrix} \end{aligned} \quad (7)$$

with the *Clarke-transformation* matrix, \mathbf{c}_t . By performing the well-known Forward-Euler method with a sampling period of T_s (time step $k \in \mathbb{N}$) on (6), the discrete-time state-space model (1) is formed with system the system matrices, $\mathbf{A}(k) = \mathbf{I}_4 + T_s \mathbf{A}_c(k)$, (where \mathbf{I}_4 is an identity matrix of size four), $\mathbf{B} = T_s \mathbf{B}_c$, and \mathbf{C} as per (7).

III. SDA BASED OPTIMIZATION

This section briefly introduces the basic formulation of the SDA, and most importantly, the suitable initialization approach to be used. As shown, thanks to the aforementioned initialization method, the computational burden of the optimization process during transients is significantly reduced.

A. Equivalent ILS Problem

The original optimization problem (3) can be used easily to compute the so-called unconstrained solution, $\mathbf{U}_{uc}(k) \in \mathbb{R}^\zeta$. Based on that, (3) is reformulated as an equivalent integer least-squares (ILS) problem [8], i.e.,

$$\mathbf{U}_{opt}(k) = \arg \min_{\mathbf{U}(k)} \|\mathbf{H}(k)\mathbf{U}(k) - \bar{\mathbf{U}}_{uc}(k)\|_2^2, \quad (8)$$

subject to (3c) and (3d). Here, $\bar{\mathbf{U}}_{uc}(k) = \mathbf{H}(k)\mathbf{U}_{uc}(k) \in \mathbb{R}^\zeta$. As derived in [2], [8], $\mathbf{H}(k) \in \mathbb{R}^{\zeta \times \zeta}$ is a non-singular lower triangular matrix (lattice generator) for $\lambda_u > 0$, and is obtained by performing the Cholesky decomposition [11] during the intermediate stage of the ILS-problem (8) formation. Once the ILS-problem has been formulated, the next step is to initialize the SDA to perform the optimization.

B. Initialization Approach

The SDA forms an initial sphere, \mathcal{S}_{ini} , with a center, Θ , and an initial radius, ρ_{ini} , based on the associated ILS-problem to be solved. This is achieved by computing ρ_{ini} , which is,

in fact, the Euclidean distance between the center Θ and an initial control input sequence, \mathbf{U}_{ini} , i.e.,

$$\mathcal{S}_{ini}(k) : \quad \rho_{ini}^2(k) = \|\mathbf{H}(k)\mathbf{U}_{ini}(k) - \Theta(k)\|_2^2. \quad (9)$$

The computational burden of the SDA depends directly on the size of initial sphere $\mathcal{S}_{ini}(k)$ and, thus, the selection of center $\Theta(k)$ and initial radius $\rho_{ini}(k)$. This $\mathcal{S}_{ini}(k)$ should be small enough containing a possibly limited number of candidate solutions in it, hence less number of computations are performed. To this end, two different initialization approach have been used in [2] depending on the location of unconstrained optimal solution $\mathbf{U}_{uc}(k)$ during the steady-state and transient operations.

According to an educated-guess initialization approach proposed in [8], the initial sphere $\mathcal{S}_{ini}(k)$ in (9) is formed by considering $\bar{\mathbf{U}}_{uc}(k)$ as the center $\Theta(k)$. Furthermore, $\mathbf{U}_{ini}(k)$ is chosen by using the previous optimal input sequence, and shifting it backwards by one time-step. This approach is particularly effective at steady-state operation, as the unconstrained solution $\mathbf{U}_{uc}(k)$ usually belongs to the *convex-hull*, $\mathbb{C}_{\mathcal{H}1}$, of the original FCS \mathbb{U} , i.e., $\mathbf{U}_{uc}(k) \in \mathbb{C}_{\mathcal{H}1}$, and it is defined as

$$\mathbb{C}_{\mathcal{H}1} = \text{Conv}(\mathbb{U}) \subset \mathbb{R}^\zeta. \quad (10)$$

As a result, usually a compact $\mathcal{S}_{ini}(k)$ results, and, thus, less computations are required. In contrast, the educated-guess initialization approach may not be a feasible option for transients, since $\mathbf{U}_{ini}(k)$ is no longer a good guess like steady-state and is far from its previous optimal. This is because the unconstrained solution $\mathbf{U}_{uc}(k)$ may be located far away from $\mathbb{C}_{\mathcal{H}1}$ ($\mathbf{U}_{uc}(k) \notin \mathbb{C}_{\mathcal{H}1}$) and thus, a larger initial sphere $\mathcal{S}_{ini}(k)$ is formed that leads to a higher number of computations.

This issue has been solved in [1] by using a box-constrained quadratic programming (QP) problem¹ that projects the infeasible $\mathbf{U}_{uc}(k) \notin \mathbb{C}_{\mathcal{H}1}$ on $\mathbb{C}_{\mathcal{H}1}$. This provides a feasible center and a relatively small initial radius for the SDA. Specifically, by solving

$$\mathbf{U}_{bc1}(k) = \arg \min_{\mathbf{U}(k)} \|\mathbf{H}(k)\mathbf{U}(k) - \bar{\mathbf{U}}_{uc}(k)\|_2^2 \quad (11a)$$

$$\text{subject to: } \mathbf{U}(k) \in \mathbb{C}_{\mathcal{H}1} \subset \mathbb{R}^\zeta \quad (11b)$$

the projected solution $\mathbf{U}_{bc1}(k)$ results. This is equivalent to $\mathbf{U}_{uc}(k)$, whenever $\mathbf{U}_{uc}(k) \in \mathbb{C}_{\mathcal{H}1}$ (generally, during the steady-state). Having found $\mathbf{U}_{bc1}(k) \in \mathbb{C}_{\mathcal{H}1}$, the new ILS-problem can be written as

$$\mathbf{U}_{sopt}(k) = \arg \min_{\mathbf{U}(k)} \|\mathbf{H}(k)\mathbf{U}(k) - \bar{\mathbf{U}}_{bc}(k)\|_2^2 \quad (12a)$$

$$\text{subject to: (3c) and (3d).} \quad (12b)$$

In (12), $\bar{\mathbf{U}}_{bc}(k) = \mathbf{H}(k)\mathbf{U}_{bc1}(k) \in \mathbb{R}^\zeta$ acts as the new center Θ for the SDA. Moreover, a feasible initial vector, $\mathbf{U}_{ini}(k) =$

¹An exterior point active set algorithm based on Lagrangian multipliers and the Karush-Kuhn-Tucker conditions is computationally feasible to solve this problem [12]–[14].

$\mathbf{U}_{\text{sq}}(k) = [\mathbf{u}_{\text{sq}}^T(k) \dots \mathbf{u}_{\text{sq}}^T(k+N-1)]^T$, is obtained when $\mathbf{U}_{\text{uc}}(k) \notin \mathbb{C}_{\mathcal{H}1}$, by sequentially quantizing $\mathbf{U}_{\text{bc}}(k)$ to \mathbb{U} , i.e.,

$$\mathbf{U}_{\text{sq}}(k) = q_{\mathbb{U}}(\mathbf{U}_{\text{bc}}(k)) \quad (13a)$$

$$\text{subject to: } \|\Delta \mathbf{u}_{\text{sq}}(\ell)\|_\infty \leq 1 \quad (13b)$$

$\forall \ell = k, \dots, k+N-1$, where $\Delta \mathbf{u}_{\text{sq}}(\ell) = \mathbf{u}_{\text{sq}}(\ell) - \mathbf{u}_{\text{sq}}(\ell-1)$, $\mathbf{u}_{\text{sq}}(k-1) = \mathbf{u}_{\text{opt}}(k-1)$ and the operator $q_{\mathbb{U}}()$ is an Euclidean vector quantizer. Here, the transition voltage level constraint (13b) in (13b) is the similar to the one considered in (3d). However, $\mathbf{U}_{\text{sq}}(k)$ differs from the so-called Babai estimation [15], [16] (also called standard quantization), by taking into account the constraint (13b). Furthermore, $\mathbf{U}_{\text{ini}}(k) = \mathbf{U}_{\text{sq}}(k)$ is chosen by using the previous optimal input. Hence, $\mathbf{U}_{\text{sq}}(k)$ is indeed a suitable $\mathbf{U}_{\text{ini}}(k)$ for transients over $\mathbf{U}_{\text{eg}}(k)$ used in [8]. Finally, the new initial sphere $\mathcal{S}_{\text{ini}}(k)$ is formed as per (9) with the new $\Theta(k) = \bar{\mathbf{U}}_{\text{bc}}(k)$, and the new $\rho_{\text{ini}}(k)$, computed by using $\mathbf{U}_{\text{ini}}(k) = \mathbf{U}_{\text{sq}}(k)$. Consequently, the computational burden of the SDA is reduced considerably with a significantly smaller $\mathcal{S}_{\text{ini}}(k)$ when solving the alternative optimal problem (12) during transients.

C. Optimization for Transient Operation

The optimization process of SDA begins by considering the selected initialization approach and a tentative solution is constructed element-by-element by performing sequential computation. This process is continued until a full-length solution is constructed and all elements are visited. In this case, the best solution is found, which is, in fact, the actual $\mathbf{U}_{\text{opt}}(k)$ in (8) or $\mathbf{U}_{\text{sopt}}(k)$ in (12). It is important to note that the SDA solves the alternative optimization problem (12) during transient operation, which in general is not equivalent to the ILS-problem (8). Thus, $\mathbf{U}_{\text{sopt}}(k)$ may be suboptimal for (8), i.e., $\mathbf{U}_{\text{sopt}}(k) \neq \mathbf{U}_{\text{opt}}(k)$. To analyze this fact, the original convex-hull $\mathbb{C}_{\mathcal{H}1}$ can be enlarged. In doing so, a smaller extension in the initial radius $\rho_{\text{ini}}(k)$ as in (9) is allowed when $\mathbf{U}_{\text{uc}}(k) \notin \mathbb{C}_{\mathcal{H}1}$ but not far (in the Euclidean sense) from $\mathbb{C}_{\mathcal{H}1}$.

A newly extended convex-hull, $\mathbb{C}_{\mathcal{H}2}$, is obtained by enlarging the FCS \mathbb{U} by one positive and negative level, i.e.,

$$\mathbb{C}_{\mathcal{H}2} = \mathbf{Conv}(\widehat{\mathbb{U}}) \subset \mathbb{R}^c \quad (14)$$

where $\widehat{\mathbb{U}} = \widehat{\mathbb{V}}^c$ and $\widehat{\mathbb{V}} = \{-2, -1, 0, 1, 2\}$.

An insight of the direct MPC problem for a transient operation that may yield a suboptimal solution is depicted in Fig. 2. In this example, an FCS \mathbb{U} of four control input vectors are represented as gray solid circles. The associated convex-hulls $\mathbb{C}_{\mathcal{H}1}$ and $\mathbb{C}_{\mathcal{H}2}$ are depicted in Fig. 2a. At time step k , the ellipses centered on the unconstrained solution $\mathbf{U}_{\text{uc}}(k)$ represent the level sets of the original optimization problem (8). Understandably, all control input vectors under an ellipse correspond to the same cost value. Therefore, the larger the Euclidean distance of an ellipse from $\mathbf{U}_{\text{uc}}(k)$ is the higher associated cost.

According to the definition of the ILS-problem ((8) or (12)), the matrix $\mathbf{H}(k)$ introduces a linear transformation of all contents in original space such as control input vectors,

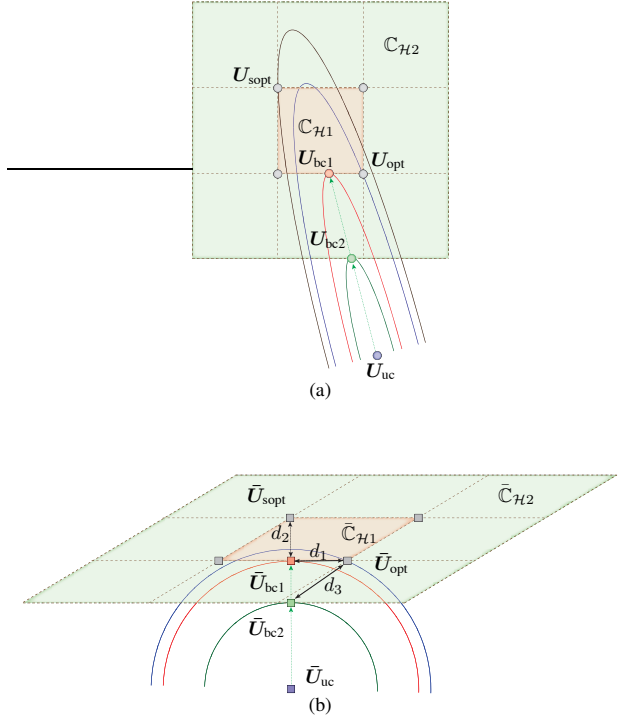


Fig. 2. Graphical representation of the direct MPC problem (an FCS \mathbb{U} of four control input vectors) in two-dimensional space for transient operation: The projection of the unconstrained solution $\mathbf{U}_{\text{uc}}(k)$ (shown as blue solid circle/ square) onto the two convex-hulls $\mathbb{C}_{\mathcal{H}1}$ and $\mathbb{C}_{\mathcal{H}2}$ in (a) the original space, and (b) the transformed space generated by \mathbf{H} .

convex-hulls, other vectors, etc, and thus, a new transformed space is generated as depicted in Fig. 2b. In this space, all ellipses are transformed into circles (spheres for larger dimensions) centered on $\bar{\mathbf{U}}_{\text{uc}}(k) = \mathbf{H}(k)\mathbf{U}_{\text{uc}}(k)$. When projecting an infeasible unconstrained solution $\mathbf{U}_{\text{uc}}(k)$ onto the boundary of $\mathbb{C}_{\mathcal{H}1}$, i.e., $\mathbf{U}_{\text{bcl}}(k)$, the SDA may lead to a suboptimal solution $\mathbf{U}_{\text{sopt}}(k)$ instead of $\mathbf{U}_{\text{opt}}(k)$ by solving (12). This scenario can be seen from Fig. 2b that $\bar{\mathbf{U}}_{\text{sopt}}(k)$ is the closed point to $\bar{\mathbf{U}}_{\text{bcl}}(k)$, i.e., $d_2 < d_1$. On the other hand, when the projection is performed on $\mathbb{C}_{\mathcal{H}2}$, the SDA finds $\mathbf{U}_{\text{opt}}(k)$ considering $\bar{\mathbf{U}}_{\text{bc2}}(k)$ as new center; the Euclidean distance d_3 between $\bar{\mathbf{U}}_{\text{bc2}}(k)$ and the optimal solution $\mathbf{U}_{\text{opt}}(k)$ is the smallest as compared with the distances from the other candidate solutions. Therefore, this analysis demonstrates the benefits of extending the convex-hull to reduce the possibility of suboptimality during transients.

IV. PERFORMANCE EVALUATION

The three-level H-bridge power inverter drives a 1.1 kW, 420 V, 50 Hz squirrel-cage IM. Consider a transient scenario where a full load step change in the torque $\mathcal{T}_l = \mathcal{T}_{e,\text{nom}} = 1$ pu is applied at 0.1 s and the controller is operated with the sampling interval $T_s = 125\mu\text{s}$. The details of the IM drive parameters, and both PI and predictive controller parameters are shown in Tables I and II, respectively.

Table I
INDUCTION MACHINE DRIVE PARAMETERS

Parameter	Symbol	SI value
dc voltage per HB	V_{dc}	300 V
dc-link capacitance	C_{dc}	3.3 mF
Rated stator frequency	$f_{s, \text{rat}}$	50 Hz
Nominal power	P_{nom}	1.1 kW
Nominal voltage	V_{nom}	420 V
Nominal current	I_{nom}	2.75 A
Nominal speed	$\omega_{m, \text{nom}}$	1400 rpm
Nominal electromagnetic torque	$T_{e, \text{nom}}$	7 Nm
Nominal rotor (flux linkage)	$\psi_{r, \text{nom}}$	1 Wb
Stator resistance	R_s	6.03 ω
Rotor resistance	R_r	6.085 ω
Stator/Rotor self-inductance	L_s / L_r	0.5192 H
Magnetizing inductance	L_m	0.4893 H
Inertia	J_m	0.011787 kg.m ²
Friction coefficient	f_m	0.017925
Number of pole pairs	n_p	2

Table II
PI AND PREDICTIVE CONTROLLER PARAMETERS

Parameter	Symbol	SI value
Predictive controller sampling time	T_s	125 μ s
Sampling time of PI $_\omega$ / PI $_f$	T_{sw}/T_{sf}	1000 μ s
Bandwidth of PI $_\omega$ / PI $_f$	BW $_\omega$ /BW $_f$	10 Hz
Discrete-time proportional gain of PI $_\omega$	$k_{p\omega}$	0.20943
Discrete-time integral gain of PI $_\omega$	$k_{i\omega}$	0.20459
Discrete-time proportional gain of PI $_f$	k_{pf}	7.66610
Discrete-time integral gain of PI $_f$	k_{if}	7.46164
Direct current (saturation)	$i_{sd, \text{sat}}$	2.044 A
Quadrature current (saturation)	$i_{sq, \text{sat}}$	3 A
Weighting factor	λ_u	0.01 – 0.3
Prediction horizon	N	1 – 10

To investigate the optimality (suboptimality) of the optimal solution with and without the proposed modification in the *convex-hull*, a measuring metric called degree of optimality, δ , is defined as

$$\delta(k) = \left\{ 1 - \frac{J_{N, \text{sopt}}(k) - J_{N, \text{opt}}(k)}{J_{N, \text{opt}}(k)} \right\} \times 100\%, \quad (15)$$

where, $J_{N, \text{opt}}(k)$ and $J_{N, \text{sopt}}(k)$ are the cost values computed for the control input obtained using the educated-guess and box-constrained QP initialization approach, respectively. Note that the cost value associated with any suboptimal solution is relatively higher than its optimal under the similar control-states of the system, i.e., $J_{N, \text{sopt}}(k) > J_{N, \text{opt}}(k)$. Therefore, $\delta(k)$ in (15) states the closeness of an obtained suboptimal solution towards its optimal one, and this metric takes up a numeric range of 0 to 100%. That means whenever $\delta(k)$ is close to 100%, $J_{N, \text{sopt}}(k) \approx J_{N, \text{opt}}(k)$ and thus, the elements in $\mathbf{U}_{\text{sopt}}(k)$ are almost similar to the elements in $\mathbf{U}_{\text{opt}}(k)$. Therefore, it can be said that for $\delta(k) = 100\%$

Table III

THE DEGREE OF OPTIMALITY $\delta(k)$ FOR THE TRANSIENT OPERATION PRESENTED IN FIG. 3, WHEN TWO DIFFERENT *Convex-hulls* $\mathbb{C}_{\mathcal{H}1}$ AND $\mathbb{C}_{\mathcal{H}2}$ ARE CONSIDERED IN THE INITIALIZATION APPROACH OF SDA. THE RESULTS ARE BASED ON SIMULATIONS AND ARE COMPUTED FOR THE PREDICTION HORIZON $N = 1$ TO 10.

N	<i>Convex-hull</i>	$\delta(k)$ [%]
1	$\mathbb{C}_{\mathcal{H}1}$	99.15
2		95.23
3		97.49
4		98.38
5		96.41
6		89.22
7		94.63
8		88.76
9		91.56
10		92.44
1-10	$\mathbb{C}_{\mathcal{H}2}$	100

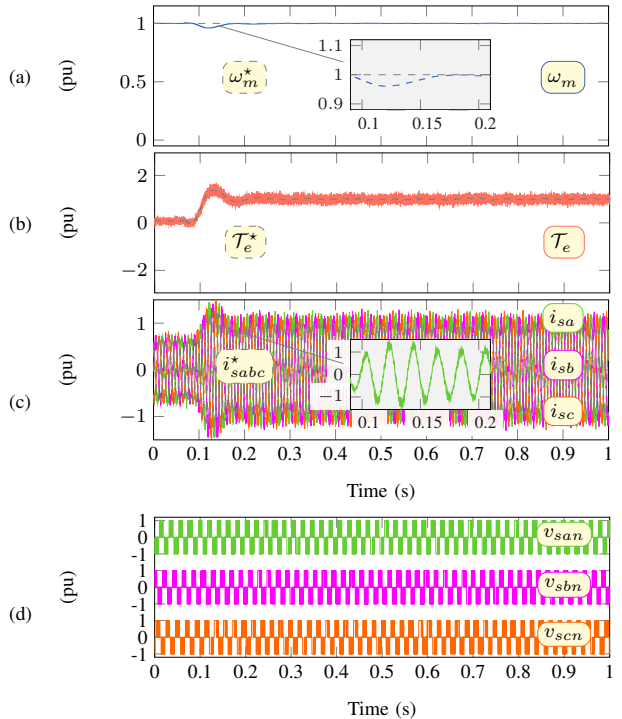


Fig. 3. Experimental transient results for $N = 4$ and *convex-hull* $\mathbb{C}_{\mathcal{H}2}$: IM is running under $\omega_m^* = \omega_{m, \text{nom}}$, $\psi_{rd}^* = \psi_{rd, \text{nom}}$, and $T_l = T_{e, \text{nom}}$ is applied at 0.1 s. (a) ω_m^* , ω_m ; (b) T_e^* , T_e ; (c) i_{sabc}^* , i_{sabc} ; and (d) inverter voltages v_{sabc} .

(i.e., $J_{N, \text{sopt}}(k) = J_{N, \text{opt}}(k)$), $\mathbf{U}_{\text{sopt}}(k)$ is exactly equivalent to $\mathbf{U}_{\text{opt}}(k)$.

Firstly, the degree of optimality $\delta(k)$ is measured by performing several simulations for prediction horizon $N = 1$ to 10 under the transient conditions mentioned above. For the SDA-based optimization, the *convex-hull* $\mathbb{C}_{\mathcal{H}1}$ is considered in the initialization approach of box-constrained QP.

Furthermore, the educated-guess initialization approach is also adopted in parallel just to compute $J_{N,\text{opt}}$, which is indeed, an optimal cost. Subsequently, $\delta(k)$ is computed for the obtained suboptimal solution during the transient operation as per (12) and presented in Table III for $N = 1$ to 10. As one can see, suboptimal solutions are frequently obtained for all N , i.e., $\delta(k) < 100\%$. Moreover, the degree of sub-optimality does not follow any pattern with respect to N .

Secondly, similar analysis is performed under the same configuration, except using the extended *convex-hull* $\mathbb{C}_{\mathcal{H}2}$. It can be stated that all tested N the optimality is maintained for the initialization approach using $\mathbb{C}_{\mathcal{H}2}$, i.e., $\delta = 100\%$. Nevertheless, this optimality can not be guaranteed always from theoretical perspective, since an alternative optimization (12) is performed when $U_{\text{uc}}(k) \notin \mathbb{C}_{\mathcal{H}2}(k)$. Consequently, the chance of obtaining suboptimal solutions are also increased.

Finally, the experimentation is performed on a dSPACE DS1106 control platform incorporated with MATLAB/Simulink with the sampling period of $T_s = 125\mu\text{s}$ and the implementation is achieved for a prediction horizon of four steps, i.e., $N = 4$. The results are shown in Fig. 3, where the machine is initially running at nominal speed $\omega_m^* = \omega_{m,\text{nom}} = 1$ pu, while considering the nominal rotor flux reference $\psi_{rd}^* = \psi_{rd,\text{nom}} = 1$ pu. Then, the transient scenario is introduced by applying a full load, i.e., $\mathcal{T}_l = \mathcal{T}_{e,\text{nom}} = 1$ pu at 0.1 s. The motor speed ω_m experiences a 4.7 % undershoot with a settling time of 6 ms, which is indeed, a natural response of the controller. Furthermore, a typical behavior of the electromagnetic torque \mathcal{T}_e and the stator currents i_{sabc} are observed in Fig. 3(b) and (c), respectively.

V. CONCLUSIONS

In this work, the impact of extending the *convex-hull* in the initialization approach of SDA during transient operation has been analyzed. With graphical explanation, it has been shown that when using the original *convex-hull* formed by the finite control set, there exists a possibility of obtaining a suboptimal solutions by the SDA during transient operation. This issue has been solved in this work by enlarging the *convex-hull* size. Thus, the probability for the SDA to maintain optimality over the whole operating regime of the system is significantly higher.

Future research will focus on a systematic design of an enlarged *convex-hull* in terms of optimality and computational effort of multistep MPC problem.

ACKNOWLEDGMENT

This research was funded in part by the Australian Government through the Australian Research Council (Discovery

Project No. DPDP180100129). This work is supported by CONICYT + FONDECYT Regular + 1191520. The work of C. A. Rojas was supported by CONICYT-PCHA/Becas-Chile/2016-74170048 and CONICYT + PAI CONVOCATORIA NACIONAL SUBVENCION A INSTALACION EN LA ACADEMIA CONVOCATORIA 2018 + PAI77180032.

REFERENCES

- [1] R. Baidya, R. P. Aguilera, P. Acuna, R. Delgado, T. Geyer, D. Quevedo, and T. Mouton, "Fast multistep finite control set model predictive control for transient operation of power converter," in *Proc. 42nd Annu. Conf. IEEE Ind. Electron. IECON'16*, Florence, Italy, Oct. 2016, pp. 5039–5045.
- [2] P. Acuna, C. Rojas, R. Baidya, R. P. Aguilera, and J. Fletcher, "On the impact of transients on multistep model predictive control for medium-voltage drives," *IEEE Trans. Power Electron.*, pp. 1–1, 2019.
- [3] P. Karamanakos, T. Geyer, and R. P. Aguilera, "Long-horizon direct model predictive control: Modified sphere decoding for transient operation," *IEEE Transactions on Industry Applications*, vol. 54, no. 6, pp. 6060–6070, Nov 2018.
- [4] J. Rodríguez, M. P. Kazmierkowski, J. R. Espinoza, P. Zanchetta, H. Abu-Rub, H. A. Young, and C. A. Rojas, "State of the Art of Finite Control Set Model Predictive Control in Power Electronics," *IEEE Trans. Ind. Informat.*, vol. 9, no. 2, pp. 1003–1016, May 2013.
- [5] T. Geyer, P. Karamanakos, and R. Kennel, "On the benefit of long-horizon direct model predictive control for drives with lc filters," in *2014 IEEE Energy Conversion Congress and Exposition (ECCE)*, Sep. 2014, pp. 3520–3527.
- [6] T. Geyer, and Quevedo, D. E., "Performance of multistep finite control set model predictive control for power electronics," *IEEE Trans. Power Electron.*, vol. 30, no. 3, pp. 1633–1644, Mar. 2015.
- [7] P. Karamanakos, T. Geyer, N. Oikonomou, F. D. Kieferndorf, and S. Manias, "Direct Model Predictive Control: A Review of Strategies That Achieve Long Prediction Intervals for Power Electronics," *IEEE Ind. Electron. Mag.*, vol. 8, no. 1, pp. 32–43, Mar. 2014.
- [8] T. Geyer and D. E. Quevedo, "Multistep Finite Control Set Model Predictive Control for Power Electronics," *IEEE Trans. Power Electron.*, vol. 29, no. 12, pp. 6836–6846, Dec. 2014.
- [9] S. Vazquez, J. I. Leon, L. G. Franquelo, J. Rodriguez, H. A. Young, A. Marquez, and P. Zanchetta, "Model Predictive Control: A Review of Its Applications in Power Electronics," *IEEE Ind. Electron. Mag.*, vol. 8, no. 1, pp. 16–31, March 2014.
- [10] P. C. Krause, O. Waszynczuk, and S. D. Sudhoff, *Analysis of Electric Machinery and Drive Systems*, 2nd ed. Hoboken, NJ, USA: Wiley, 2002.
- [11] R. B. Schnabel and E. Eskow, "A new modified cholesky factorization," *SIAM J. Sci. and Stat. Comput.*, vol. 11, no. 6, pp. 1136–1158, 1990.
- [12] S. Bubeck, *Convex Optimization: Algorithms and Complexity*. Now Foundations and Trends, 2015.
- [13] S. Boyd and L. Vandenberghe, *Convex Optimization*. Cambridge, UK: Cambridge Univ. Press, 2004.
- [14] J. J. Mor and G. Toraldo, "On the solution of large quadratic programming problems with bound constraints," *SIAM Journal on Optimization*, vol. 1, no. 1, pp. 93–113, 1991.
- [15] L. Babai, "On lovász lattice reduction and the nearest lattice point problem," *Combinatorica*, vol. 6, no. 1, pp. 1–13, 1986.
- [16] P. Karamanakos, T. Geyer, T. Mouton, and R. Kennel, "Computationally efficient sphere decoding for long-horizon direct model predictive control," in *IEEE Energy Conversion Congress and Exposition (ECCE)*, Sep. 2016, pp. 1–8.